Model for classical and ultimate regimes of radiatively driven turbulent convection.

Mathieu Creyssels

▶ **To cite this version:**

Mathieu Creyssels. Model for classical and ultimate regimes of radiatively driven turbulent convection.. Journal of Fluid Mechanics, 2020, 900, 10.1017/jfm.2020.521 . hal-02299927v2

HAL Id: hal-02299927
https://hal.science/hal-02299927v2

Submitted on 15 Jun 2020

HAL is a multi-disciplinary open access archive for the deposit and dissemination of scientific research documents, whether they are published or not. The documents may come from teaching and research institutions in France or abroad, or from public or private research centers.

L'archive ouverte pluridisciplinaire **HAL**, est destinée au dépôt et à la diffusion de documents scientifiques de niveau recherche, publiés ou non, émanant des établissements d'enseignement et de recherche français ou étrangers, des laboratoires publics ou privés.

Model for classical and ultimate regimes of radiatively driven turbulent convection

M. Creyssels†

Laboratoire de Mécanique des Fluides et d'Acoustique, Ecole Centrale de Lyon, Univ. Lyon, CNRS, 69134 Ecully, France

(Received xx; revised xx; accepted xx)

In a standard Rayleigh-Bénard experiment, a layer of fluid is confined between two horizontal plates and the convection regime is controlled by the temperature difference between the hot lower plate and the cold upper plate. The effect of direct heat injection into the fluid layer itself, for example by light absorption, is studied here theoretically. In this case, the Nusselt number (Nu) depends on three non-dimensional parameters: the Rayleigh (Ra) and Prandtl (Pr) numbers and the ratio between the spatial extension of the heat source (l) and the height of the fluid layer (h). For both the well known classical and ultimate convection regimes, the theory developed here gives a formula for the variations of the Nusselt number as a function of these parameters. For the classical convection regime, by increasing l/h from 0 to 1/2, Nu gradually changes from the standard scaling $Nu \sim Ra^{1/3}$ to an asymptotic scaling $Nu \sim Ra^{\theta}$, with $\theta = 2/3$ or $\theta = 1$ by adopting, respectively, the Malkus (1954) theory or the Grossmann & Lohse (2000) theory. For the ultimate convection regime, Nu gradually changes from $Nu \sim Ra^{1/2}$ scaling to an asymptotic behaviour seen only at very high Ra for which $Nu \sim Ra^{2}$. This theory is validated by the recent experimental results given by Bouillaut *et al.* (2019) and also shows that for these experiments, Ra and Re numbers were too small to observe the ultimate regime. The predictions for the ultimate regime cannot be confirmed at this time due to the absence of experimental or numerical work on convection driven by internal sources and for very large Ra numbers.

1. Introduction

Rayleigh-Bénard (RB) convection is a classical fluid dynamics problem and has been the subject of numerous experimental, theoretical and numerical studies. When Rayleigh numbers are high (generally above 10^6), two distinct theories, called classical and ultimate, give two distinct asymptotic behaviours for the Nusselt number as a function of the Rayleigh number. The classical theory states that the heat flux should be independent of the height of the fluid layer leading from the definition of Nu and Ra to the following asymptotic law: $Nu \sim Ra^{1/3}$ (Malkus 1954; Priestley 1954; Grossmann & Lohse 2000). The ultimate theory asserts that for very high Rayleigh numbers, the heat flux should become independent of the fluid dissipative coefficients ν and κ giving an asymptotic law like $Nu \sim Ra^{1/2}$ (Kraichnan 1962; Spiegel 1971; Siggia 1994; Chavanne *et al.* 1997; Ahlers *et al.* 2009; Grossmann & Lohse 2011; Chillà & Schumacher 2012).

This paper is an extension of RB theories in the case of a heat source spatially distributed within the fluid layer. An example of this kind of heating is given by Lepot *et al.* (2018); Bouillaut *et al.* (2019). The authors experimentally developed a new RB cell concept for which heat is not injected through thermal conduction between the lower

† Email address for correspondence: mathieu.creyssels@ec-lyon.fr

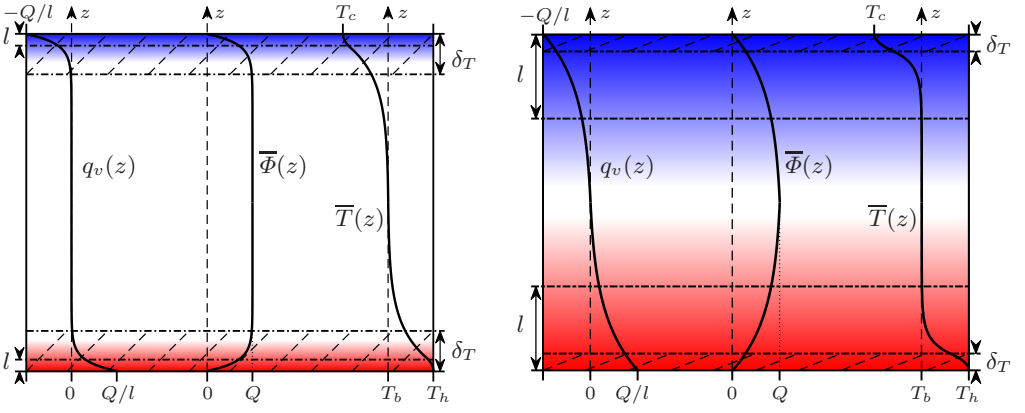

FIGURE 1. Modified RB experiment in the case of $l/\delta_T < 1$ (left) and in the case of $l/\delta_T > 1$ (right). The heat is injected in volume near the lower plate (red zone) while the fluid is cooled in volume near the upper plate (blue area), both with a characteristic length l. The two thermal boundary layers with a width of δ_T are also displayed (hatched areas). The profiles of the volumetric (positive and negative) power source (q_v), the mean heat flux ($\overline{\Phi}$) and the mean temperature ($\overline{T}$) are also shown for each case.

heating plate and the fluid above it. In their experiment, the lower plate is transparent and the working fluid is a homogeneous mixture of water and dye. A powerful spotlight placed under the lower plate shines through the fluid, and the light, after passing through the transparent plate, is absorbed by dye and therefore by the fluid located near the plate. According to the Beer-Lambert law, this kind of heating corresponds to a volume heat source that decays exponentially from the lower plate to a characteristic height l, leading to a local heating of the following form:

$$q_v(z) = \frac{Q}{l} \exp\left(-\frac{z}{l}\right), \tag{1.1}$$

where Q is the total heat flux radiated by the spotlight into the fluid (in $\mathrm{W/m^2}$) and z is the vertical coordinate with $z = 0$ on the lower plate. The characteristic height l can be changed since it is inversely proportional to the dye concentration. Hereafter, (1.1) is assumed to be valid even if the model proposed in this article can easily be generalized to other forms of local heating rates.

Lepot *et al.* (2018); Bouillaut *et al.* (2019) and Doering (2019) claimed that the study of this type of modified RB experiments should allow progress in understanding turbulent convection in both natural flows and a conventional RB cell. Indeed, in many geophysical and astrophysical flows, convection is driven by internal heating due to, for example, the radioactive decay in the Earth's mantle or the thermonuclear reactions in stars. It is therefore easy to understand that a modified RB experiment is a first approach to model turbulent flows in natural systems even if Ra numbers are very different. In addition this work also aims to provide interesting information on turbulent convection. Indeed, heat transport in a conventional RB cell is essentially controlled by the thermal boundary layers near the plates and their stability explains the difference between the two theories of convection (the classical and the ultimate). To investigate these boundary layers, the location of the heat sources can be easily changed by adjusting the absorption height l (Lepot *et al.* 2018; Bouillaut *et al.* 2019). This is a similar approach to that used by other authors, which consists of replacing the lower and upper plates with rough plates (Shen *et al.* 1996; Roche *et al.* 2001; Qiu *et al.* 2005; Stringano *et al.* 2006; Tisserand

et al. 2011; Zhu *et al.* 2017, 2019). Roche *et al.* (2001) and Tisserand *et al.* (2011) reported an increase of the Nu vs Ra scaling exponent from 1/3 to 1/2, even if the range of Ra explored and their interpretation of it was very different. Roche *et al.* (2001) interpreted the transition for the exponent to the value 1/2 as a turbulent transition for the thermal boundary layers because the Ra numbers were high ($> 10^{12}$) and the transition was already observed with smooth plates. On the contrary, Tisserand *et al.* (2011) interpreted the increase in the exponent as a destabilization by buoyancy of the fluid placed between the rough elements. The observation of the exponent 1/2 is then fortuitous in the latter case and, as underlined by Zhu *et al.* (2017); Rusaouën *et al.* (2018), the exponent 1/2 can only be seen over a limited range of the Rayleigh number. By increasing Ra further, the exponent decreases and returns to its classical value close to 1/3. Note that the range of Ra for which exponent 1/2 is observed can be increased using multi-scale roughness (Zhu *et al.* 2019).

In this theoretical study, a model is proposed to deduce scaling laws of the Nusselt number as a function of the three non-dimensional parameters that control turbulent convection *i.e.* Ra, Pr and the ratio of absorption height to cell height ($\tilde{l} = l/h$). In a standard RB experiment, both plates play the same role (for a small temperature difference and by adopting the Boussinesq approximation) and the corresponding thermal boundary layers have the same behaviour and therefore the same width (δ_T). To have two similar boundary layers in a modified RB cell, the upper part of the cell must be cooled with the same power profile as that used for the heating process, so $q_v(z) = -\frac{Q}{l}\exp(-\frac{h-z}{l})$. The injected or extracted power profile is shown in Fig. 1 for both cases $l/\delta_T < 1$ (left) and $l/\delta_T > 1$ (right). When $l \to 0$, this experiment becomes a standard RB experiment while, when the length l increases, the lower and upper thermal boundary layers are heated and cooled respectively. Finally, when l becomes greater than δ_T, the bulk flow is also heated and cooled simultaneously since the lower region is heated while the upper region is cooled (Fig. 1 right). The Rayleigh number in a modified RB experiment can be defined as in a conventional RB cell by using the temperature difference between the two plates ($\Delta T = T_h - T_c$), between the lower plate and the mean bulk flow ($\Delta T = 2(T_h - T_b)$) or between the mean bulk flow and the upper plate ($\Delta T = 2(T_b - T_c)$). When Rayleigh numbers are high, it is assumed that the convective flow of a modified RB experiment is strong enough to impose an almost constant mean temperature over time in the bulk flow, *i.e.* outside the boundary layers (see Fig. 1), as experimentally observed in a standard RB experiment.

A major difference between modified and standard RB experiments concerns the mean heat flux through the cell from the bottom plate to the top plate. Indeed, when a steady state is reached, the heat flux averaged over a horizontal section must be independent of the vertical coordinate (z) for a standard RB experiment, whereas for a modified RB cell, this heat flux cannot be constant even in a steady state. When considering a horizontal slice of fluid, the energy given in volume must be evacuated outside the slice, which requires a gradient of the mean heat flux in the fluid (see Fig. 1). For $z = 0$ and $z = h$, the heat flux is zero because the two horizontal plates are assumed to be perfectly insulated. Far from the plates, in the center of the cell where $l \ll z \ll h - l$, the volumetric heat source q_v is close to 0, and energy conservation leads to a heat flux equal to $Q\vec{e}_z$. Thus, with the exception of the blue and red regions shown in Fig. 1, Q represents the heat flux through the cell and the Nusselt number can be defined as in a standard RB experiment as

$$Nu = \frac{Qh}{\lambda \Delta T}, \tag{1.2}$$

where λ is the thermal conductivity of the fluid and h the height of the cell. As previously mentioned, when $\tilde{l} \to 0$, Nu tends towards the Nusselt number that can be obtained in the same cell but with standard RB conditions that are a constant heat flux and fixed temperatures at both plates. Hereafter, this Nusselt number will be taken as a reference and called $Nu_0(Ra, Pr) = \lim_{\tilde{l}\to 0} Nu(Ra, Pr, \tilde{l})$.

Finally, it is questionable whether this type of modified RB experiment can be performed experimentally. Indeed, heating in volume can be achieved using either strong light (Lepot *et al.* (2018)), an electric current or even by fixing heating elements in the fluid (Kulacki & Goldstein (1972); Goluskin (2015); Goluskin & van der Poel (2016)). On the contrary, cooling in volume is more difficult to achieve experimentally. However, Lepot *et al.* (2018); Bouillaut *et al.* (2019) have shown that, in their experiments, turbulent convection develops quasi-stationary internal temperature gradients leading to a temperature difference between the lower plate and the bulk flow that is almost constant over time (see Fig. 1 B in Lepot *et al.* (2018)). Therefore, the theoretical results given below will be compared in section 4 with those obtained experimentally by Lepot *et al.* (2018); Bouillaut *et al.* (2019). The theoretical model is based, on the one hand, on the known structure of the flow and temperature fields observed experimentally and numerically in a standard RB cell at high Rayleigh numbers (generally $> 10^6$), on the other hand, on the different theories of RB convection given in the literature.

2. Background on Nu vs Ra scalings for standard RB convection

For high Rayleigh numbers, convective flow is turbulent almost everywhere in the cell except in two thin thermal boundary layers located against the lower and upper plates. This dynamic structure of the flow yields to a particular field for the mean temperature. Indeed, in the bulk flow, turbulent convection produces large temporal and spatial variations for temperature fluctuations but an almost uniform mean temperature field with $\overline{T}_b = (T_h + T_c)/2$ for symmetry reasons and assuming the Boussinesq approximation is valid (the mean temperature profile is represented in Fig. 1). On the contrary, the mean temperature increases or decreases by $\Delta T/2 = (T_h - T_c)/2$ in each boundary layer. Therefore, the heat transfer averaged over a horizontal section is dominated by turbulent convection in the bulk flow ($\overline{\Phi} \approx \rho c_p \overline{w'T'}$, where w' and T' are the fluctuations of the vertical velocity and temperature respectively), whereas the heat transfer is driven by thermal conduction in the two thin boundary layers ($\overline{\Phi} \approx -\lambda \partial \overline{T}/\partial z$, where $\overline{T}(z)$ is the temperature averaged both on time and on a horizontal section located at the distance z from the plate). The thickness of each thermal boundary layer (δ_T) is controlled by the temperature difference $\Delta T/2$ and the mean heat flux assuming that $\overline{\Phi}$ can be written as $\overline{\Phi} = \lambda \Delta T/(2\delta_T)$. This last equation is valid regardless of the convection regime or the adopted theory (see Kraichnan (1962) and Grossmann & Lohse (2000)), leading to a ratio δ_T/h depending only on the Rayleigh number as

$$\frac{\delta_T}{h} = \frac{1}{2Nu_0(Ra, Pr)}. \tag{2.1}$$

2.1. *Classical regime by Malkus (1954)*

The first regime of convection, called classical, was proposed by Malkus (1954); Priestley (1954). It has the merit of simplicity and predicts a scaling law $Nu_0 \sim Ra^{1/3}$, hence with an exponent 1/3 close to the exponents observed both in the experiments and the numerical simulations in the range of Ra between 10^6 and 10^{12}. This regime of convection is entirely characterized by a constant Rayleigh number for each boundary

layer as:

$$\frac{g\alpha\Delta T\delta_T^3}{2\nu\kappa} = Ra^*. \tag{2.2}$$

Using (2.1) and (2.2), we obtain for the classical regime:

$$Nu_0 = \left(\frac{Ra}{2^4 Ra^*}\right)^{1/3}. \tag{2.3}$$

2.2. *Ultimate regime by Kraichnan (1962)*

For very large Rayleigh numbers, the thermal boundary layers observed in the case of the classical regime can be destabilized and Kraichnan (1962); Spiegel (1971) assumed that they could become similar to the velocity boundary layers observed in the case of a fully developed mean shear flow. This ultimate regime is then characterized by a constant but Prandtl-dependent Péclet number for each thermal boundary layer:

$$\frac{v_0^*\delta_T}{\kappa} = Pe^*(Pr), \tag{2.4}$$

where $\kappa = \lambda/(\rho c_p)$ is the thermal diffusivity of the fluid. For small Prandtl numbers, the thickness of the viscous sublayer is smaller than δ_T leading to a constant Péclet number $Pe^* = Pe^*_{Pr\to 0}$. On the contrary, at moderate Pr numbers, Pe^* varies as $\sqrt{Pr}$ since $Pe^* = \sqrt{Pe^*_{Pr\to 0} Re_s Pr}$, where Re_s is the characteristic Reynolds number for the top of the viscous sublayer (Kraichnan 1962). The new unknown parameter v_0^* can be interpreted as a friction velocity and measures the rms value of velocity fluctuations at the edge of each boundary layer, similarly to the friction velocity defined in the case of a channel flow. Unlike the classical regime for which the characteristic Rayleigh number Ra^* depends only on ΔT and δ_T, Pe^* is linked to the convective flow in the bulk by the velocity fluctuations v_0^*. Thus, determining the Nusselt number for the ultimate regime requires additional assumptions and equations. The parameter v_0^* is an increasing function of the large-scale mean velocity (U_0), also called as the wind turbulence. By analogy with what is well known for the channel flow, Kraichnan (1962) assumed that $v_0^* \sim U_0/\ln Re_0$, with $Re_0 = U_0 h/\nu$. In addition, the wind velocity is obtained by writing that the Richardson number in the bulk flow is of order 1, *i.e.* $Ri = g\alpha(\overline{w'T'})h/U_0^3 \sim 1$. Using the definitions of Re_0, Ra and Nu_0, this last equation yields to

$$Re_0^3 \sim \frac{RaNu_0}{Pr^2}. \tag{2.5}$$

We can note that (2.5) is valid both for the classical regime obtained by Malkus (1954), the ultimate regime proposed by Kraichnan (1962), and the two convection regimes (II and IV) of the Grossmann & Lohse (2000) theory (see section 2.3). Using (2.1), (2.5) and $v_0^* \sim U_0/\ln Re_0$, (2.4) becomes

$$Re_0^2 \ln(Re_0) \sim \frac{Ra}{PrPe^*}. \tag{2.6}$$

Then, using (2.6), (2.5) gives the Nusselt number for the ultimate regime:

$$Nu_0 \sim \left(\frac{Pr\,Ra}{[Pe^*\ln(Re_0)]^3}\right)^{1/2}. \tag{2.7}$$

For small Pr numbers (typically $Pr < Pe^*_{Pr\to 0}/Re_s$), $Nu_0 \sim Pr^{1/2}Ra^{1/2}/(\ln Re_0)^{3/2}$ while for moderate Pr numbers, $Nu_0 \sim Pr^{-1/4}Ra^{1/2}/[\ln(Re_0)]^{3/2}$.

2.3. *RB theory by Grossmann & Lohse (2000)*

Grossmann & Lohse (2000) (GL) proposed a RB theory to describe with more precision the Rayleigh and Prandtl dependence of the Nusselt number. The kinetic energy and thermal dissipation rates which are defined respectively as $\epsilon_u = \frac{\nu}{2}\sum_{i,j}(\partial_j u_i + \partial_i u_j)^2$ and $\epsilon_T = \kappa\sum_i(\partial_i T)^2$ play a central role in GL theory. In steady state and averaging over the whole RB cell the two equations of conservation of the turbulent kinetic energy ($\frac{1}{2}\sum_i u_i^2$) and of the square of the temperature give the following two exact relations:

$$\langle\epsilon_u\rangle = \frac{\nu^3}{h^4}\frac{(Nu_0 - 1)Ra}{Pr^2}, \tag{2.8}$$

$$\langle\epsilon_T\rangle = \kappa\left(\frac{\Delta T}{h}\right)^2 Nu_0. \tag{2.9}$$

The key idea of the GL theory is to split both mean dissipation rates into two contributions each, one from the bulk (Bu) and one from the boundary layers (BLs) as

$$\langle\epsilon_u\rangle = \langle\epsilon_u\rangle_{Bu} + \langle\epsilon_u\rangle_{BL}, \tag{2.10}$$

$$\langle\epsilon_T\rangle = \langle\epsilon_T\rangle_{Bu} + \langle\epsilon_T\rangle_{BL}, \tag{2.11}$$

where

$$\langle\epsilon_u\rangle_{Bu} = \frac{1}{h}\int_{\delta_u}^{h-\delta_u}\overline{\epsilon_u}(z)\mathrm{d}z \quad \text{and} \quad \langle\epsilon_T\rangle_{Bu} = \frac{1}{h}\int_{\delta_T}^{h-\delta_T}\overline{\epsilon_T}(z)\mathrm{d}z \tag{2.12}$$

are, respectively, the viscous and thermal dissipation taking place in the bulk flow. Whereas the viscous and thermal dissipation taking place in the boundary layers can be written as:

$$\langle\epsilon_u\rangle_{BL} = \frac{2}{h}\int_{0}^{\delta_u}\overline{\epsilon_u}(z)\mathrm{d}z \quad \text{and} \quad \langle\epsilon_T\rangle_{BL} = \frac{2}{h}\int_{0}^{\delta_T}\overline{\epsilon_T}(z)\mathrm{d}z. \tag{2.13}$$

In (2.12) and (2.13), the kinetic energy and thermal dissipation rates are first averaged over a horizontal cross-section giving $\overline{\epsilon_u}$ and $\overline{\epsilon_T}$, respectively. The thickness of the thermal BLs (δ_T) is given by (2.1) while a Blasius-type layer is assumed for the viscous BLs, with a thickness of

$$\frac{\delta_u}{h} = \frac{a}{\sqrt{Re_0}}. \tag{2.14}$$

Note that the prefactor a is obtained by match with a record of experimental results (Stevens *et al.* 2013).

To obtain the Rayleigh dependence of the Nusselt and Reynolds numbers, $\overline{\epsilon_u}$ and $\overline{\epsilon_T}$ need to be estimated both in the bulk flow and in the BLs:

$$\langle\epsilon_u\rangle_{Bu} \sim \frac{U_0^2}{h/U_0}\left(1 - \frac{\delta_u}{h}\right) \approx \frac{\nu^3}{h^4}Re_0^3, \tag{2.15}$$

$$\langle\epsilon_T\rangle_{Bu} \sim \frac{(\Delta T)^2}{h/U_0^{edge}}\left(1 - \frac{\delta_T}{h}\right) \approx \kappa\left(\frac{\Delta T}{h}\right)^2 Re_0 Prf\left(\frac{2aNu_0}{\sqrt{Re_0}}\right), \tag{2.16}$$

$$\langle\epsilon_u\rangle_{BL} \sim \nu\left(\frac{U_0}{\delta_u}\right)^2\frac{\delta_u}{h} = \frac{\nu^3}{h^4}\frac{Re_0^{5/2}}{2a}, \tag{2.17}$$

$$\langle\epsilon_T\rangle_{BL} \sim \kappa\left(\frac{\Delta T}{\delta_T}\right)^2\frac{\delta_T}{h} = 2\kappa\left(\frac{\Delta T}{h}\right)^2 Nu_0. \tag{2.18}$$

In (2.16), the relevant velocity at the edge between thermal BL and the thermal bulk can be less than U_0, depending on the ratio: $\delta_u/\delta_T = 2aNu_0/\sqrt{Re_0}$. Grossmann & Lohse

(2001) introduced a function $0 \leqslant f \leqslant 1$ saying that the relevant velocity at the edge then becomes $U_0^{edge} = U_0 f(\delta_u/\delta_T)$, with $f \to 1$ when $\delta_u/\delta_T \to 0$ and $f \to 0$ for $\delta_u \gg \delta_T$. They gave $f(x) = (1 + x^n)^{-1/n}$, with $n = 4$ as an example of function f.

Grossmann & Lohse (2001) have also extended those estimations of the viscous and dissipation rates for very large Prandtl numbers for which (2.14) cannot stay valid. Indeed, when Pr is high enough, δ_u must saturate to a maximum value $\delta_u(Re_c)$ lower than the height of the cell. The critical Reynolds number Re_c was estimated from experimental data to 0.28 by Grossmann & Lohse (2001) and 0.35 by Stevens *et al.* (2013). However, for the sake of simplicity, only the case of $Re_0 \gg Re_c$ is considered here.

From decomposition of the two global dissipation rates (2.10) and (2.11), four regimes of convection can be defined depending on whether the bulk or the BL contributions dominate the global dissipations. Besides, each of these four regimes is in principle divided into two subregimes, depending on whether the thermal BL or the kinetic BL is larger. The two $\langle\overline{\epsilon_u}\rangle_{Bu}$ bulk-dominated regimes (referred to as II and IV) are first presented because most of the experimental and numerical results fall under one of these two regimes (see figure 8 from Stevens *et al.* (2013)).

2.3.1. *Regimes II and IV, $\langle\epsilon_u\rangle \sim \langle\epsilon_u\rangle_{Bu}$*

For regimes II and IV, the kinetic energy dissipation rate is dominated by its bulk contribution. Combining (2.8) and (2.15), and assuming $Nu_0 \gg 1$, we obtain (2.5) again. Regime IV is obtained for high Ra numbers for which thermal dissipation rate is dominated by its bulk contribution. Combining (2.9) and (2.16), it yields to:

$$Nu_0 \sim Re_0 Pr f\left(\frac{2aNu_0}{\sqrt{Re_0}}\right) \quad \text{(Regime } IV\text{)}. \tag{2.19}$$

For lower Ra numbers, the thermal dissipation rate is dominated by its BL contribution. However, combining (2.9) and (2.18) yields to a trivial equation for Nu_0. To obtain a scaling relation between Nu_0 and Re_0, Grossmann & Lohse (2000) proposed to consider, in each thermal BL, the order of magnitude of the different terms of energy equation:

$$u_x \partial_x T + u_z \partial_z = \kappa \partial_{zz} T. \tag{2.20}$$

Both terms on the left-hand side are of order $U_0^{edge}\Delta T/h$ whereas $\kappa\partial_{zz}T \sim \kappa\Delta T/\delta_T^2$. Hence, using (2.1), one gets

$$Nu_0 \sim \sqrt{Re_0 Pr f\left(\frac{2aNu_0}{\sqrt{Re_0}}\right)} \quad \text{(Regime } II\text{)}. \tag{2.21}$$

Combining (2.5) and (2.19) or else (2.5) and (2.21), we obtain:

$$Nu_0^{\theta_i} \sim (Nu_0 RaPr)^{1/3} f\left[\frac{2a(Nu_0 RaPr)^{1/3}}{(Ra/Nu_0)^{1/2}}\right], \text{ with } \theta_{II} = 2 \text{ and } \theta_{IV} = 1. \tag{2.22}$$

For Prandtl numbers small or large enough, $f(x) \approx 1$ ($\delta_T \gg \delta_u$) or $f(x) \approx 1/x$ ($\delta_u \gg \delta_T$), and (2.22) can be simplified as follows:

$$Nu_0 \sim \begin{cases} (RaPr)^{1/(3\theta_i - 1)}, \text{ for } \delta_T \gg \delta_u, & (2.23a) \\ Ra^{1/(2\theta_i + 1)}, \text{ for } \delta_u \gg \delta_T. & (2.23b) \end{cases}$$

We can note that the sub-regime IV_u ($\delta_u \gg \delta_T$) gives the same scaling as predicted by Malkus (1954), i.e $Nu_0 \sim Pr^0 Ra^{1/3}$.

2.3.2. *Regimes I and III,* $\langle\epsilon_u\rangle \sim \langle\epsilon_u\rangle_{BL}$

For these two regimes, (2.5) needs to be replaced by

$$Re_0^{5/2} \sim \frac{RaNu_0}{Pr^2}. \tag{2.24}$$

Equation (2.24) is obtained by combining (2.8) and (2.17). As for regime IV, thermal dissipation rate is dominated by its bulk contribution in regime III and (2.19) is valid. On the contrary, in regime I, we use (2.21) instead of (2.19), as for regime II. The Ra- and Pr-dependent Nusselt number is then given by

$$Nu_0^{\theta_i} \sim (Nu_0 Ra\sqrt{Pr})^{2/5} f\left\{\frac{2a(Nu_0 Ra\sqrt{Pr})^{2/5}}{[Ra^3/(Nu_0^2 Pr)]^{1/5}}\right\}, \text{ with } \theta_I = 2 \text{ and } \theta_{III} = 1. \tag{2.25}$$

For Prandtl numbers small or large enough, (2.25) becomes:

$$Nu_0 \sim \begin{cases} (Ra\sqrt{Pr})^{2/(5\theta_i-2)}, \text{ for } \delta_T \gg \delta_u, & (2.26a) \\ Ra^{3/(5\theta_i+2)} Pr^{-1/(5\theta_i+2)}, \text{ for } \delta_u \gg \delta_T. & (2.26b) \end{cases}$$

2.3.3. *Grossmann & Lohse (2001) theory for the whole parameter* (Ra, Pr) *plane.*

The 4 previous regimes can only be observed experimentally and numerically for extreme values of Ra and Pr numbers. For instance regime IV corresponds to very high Ra numbers but in this case ultimate convection could appear while regime II is valid only for very small Ra numbers for which convection is not really turbulent. Grossmann & Lohse (2001) proposed to describe convection at any Ra and Pr numbers as a mixture of these 4 regimes. By replacing the expressions of $\langle\epsilon_u\rangle_{Bu}$ (2.15) and $\langle\epsilon_u\rangle_{BL}$ (2.17) in the balance equation for the viscous dissipation rate (2.10), they obtained this first generalised equation:

$$\frac{RaNu_0}{Pr^2} = c_1 \frac{Re_0^{5/2}}{2a} + c_2 Re_0^3. \tag{2.27}$$

Using (2.19) and (2.21), the second generalised equation can be written as:

$$Nu_0 = c_3 \sqrt{Re_0 Pr f\left(\frac{2aNu_0}{\sqrt{Re_0}}\right)} + c_4 Re_0 Pr f\left(\frac{2aNu_0}{\sqrt{Re_0}}\right). \tag{2.28}$$

Equations (2.27) and (2.28) give the dependency in Ra and Pr of both Re_0 and Nu_0 numbers, assuming the 5 coefficients (a,c_1-c_4) are known. Stevens *et al.* (2013) determined these coefficients from previous experimental measurements in the literature.

3. Nu vs Ra scalings for internal source driven convection

Using the assumptions discussed below, the Nu *vs* Ra scalings presented in previous section for standard RB experiments are generalized for the modified experiments described in the introduction and in figure 1. The basic assumption is to state that, for high Ra numbers, the dynamical structure of the convective flow is the same in the standard and modified RB experiments. At a constant Ra number, heating in volume produces the same type of thermal boundary layers as those observed in a standard RB cell. The increase in the power of the heating and cooling sources results in an increase in the bulk flow temperature, but the two types of convection experiments are so similar and the mechanisms that control the convective flow are so robust that for both classical and

ultimate regimes, the values of Ra^* and Pe^* are identical in both types of experiments. For the GL theory, the a parameter and the 4 dimensionless prefactors (1 by regime) are assumed to be independent of the experiment under consideration.

Secondly, in steady state, the equation of heat averaged over a horizontal section can be written as

$$\frac{\mathrm{d}(\overline{w'T'})}{\mathrm{d}z} - \lambda \frac{\mathrm{d}^2\overline{T}}{\mathrm{d}z^2} = q_v(z). \tag{3.1}$$

The internal heating and cooling sources are balanced either by convective flux in the bulk flow or by a conductive flux in both boundary layers. Hereafter, only the lower boundary layer will be considered since the upper boundary layer has the same behaviour. In the boundary layer, by neglecting the convective term and using the expression of $q_v(z)$ (see 1.1), (3.1) can be integrated twice to obtain:

$$T_h - \overline{T}(z) = \frac{Qh}{\lambda}\left\{\frac{z}{h} - \frac{l}{h}[1-\exp(-z/l)]\right\}. \tag{3.2}$$

For $z = \delta_T$ and using the definition of the Nusselt number (1.2), (3.2) yields to

$$\frac{1}{2Nu} = \frac{\delta_T}{h} - \frac{l}{h}[1-\exp(-\delta_T/l)]. \tag{3.3}$$

3.1. *Extension of the classical regime given by Malkus*

In the classical regime by Malkus, (2.2) yields to

$$\frac{\delta_T}{h} = \left(\frac{2Ra^*}{Ra}\right)^{1/3} = \frac{1}{2Nu_0}. \tag{3.4}$$

Using (3.4), (3.3) becomes

$$\frac{Nu}{Nu_0} = \frac{1}{1 - 2\,\tilde{l}\,Nu_0\left[1-\exp\left(-\frac{1}{2\,\tilde{l}\,Nu_0}\right)\right]}. \tag{3.5}$$

In (3.4) and (3.5), Nu_0 is the Nusselt number for a standard RB experiment in the classical regime but it also represents the limit of Nu when $\tilde{l} = l/h \to 0$. Even if Nu depends on both parameters $\tilde{l}$ and Ra, Eq. (3.5) shows that the Nusselt ratio Nu/Nu_0 is a function of a single variable that is the product of $\tilde{l}$ and Nu_0. This is the main result of the present theory and is tested against experimental results in section 4.

The limits of (3.5) when $\tilde{l} \to 0$ and $\tilde{l}Nu_0 \gg 1$ are given in Table 1. It can be noted that, when the product of $\tilde{l}$ and Nu_0 increases from 0 to ∞, the Ra-dependent Nusselt number (Nu) increases from a power law of one third to a two thirds, *i.e.* with an exponent greater than 1/2 which characterizes the ultimate regime for a standard RB experiment (Eq. 2.7).

3.2. *Extension of the Kraichnan's ultimate regime*

Unlike the classical regime for which the thickness of the boundary layers depends only on Ra whatever the type of experiment considered (see (3.4)), Eq. (2.4) shows that, in the ultimate regime, δ_T depends on the velocity fluctuations in the bulk (v^*) and therefore on the thermal power injected into the bulk flow. Assuming as before that $v^* \sim U/\ln Re$ (Kraichnan 1962), (2.4) becomes for a modified RB experiment

$$\frac{\delta_T}{h} = \frac{Pe^*}{Pr}\frac{\ln(Re)}{Re} = \frac{(\delta_T)_0}{h}\frac{Re_0}{\ln(Re_0)}\frac{\ln(Re)}{Re}. \tag{3.6}$$

For a standard RB experiment, $(\delta_T)_0$ is given by (2.1) and thus (3.6) becomes

$$\frac{\delta_T}{h} = \frac{1}{2Nu_0}\frac{Re_0}{Re}\left[1 + \frac{\ln(Re/Re_0)}{\ln(Re_0)}\right]. \tag{3.7}$$

As assumed previously for standard RB experiments, the Richardson number in the bulk flow is taken of order 1 *i.e.* $Ri = g\alpha(\overline{w'T'})h/U^3 = g\alpha\kappa Qh/(\lambda U^3) \sim 1$ yielding to $Re^3 \sim RaNu/Pr^2$, similarly to (2.5). Therefore, at constant Rayleigh number, the ratio of the Reynolds numbers for standard and modified RB experiments is proportional to the one-third power law of the ratio of the Nusselt numbers

$$\frac{Re}{Re_0} = \left(\frac{Nu}{Nu_0}\right)^{1/3}. \tag{3.8}$$

Furthermore, (3.8) is valid both for ultimate and classical regimes of convection. Using (3.7) and (3.8), (3.3) can be written as

$$\mathcal{N}^2 = \frac{1}{1+\alpha - 2\tilde{l}Nu_0\mathcal{N}\left[1-\exp\left(-\frac{1+\alpha}{2\tilde{l}Nu_0\mathcal{N}}\right)\right]}, \tag{3.9}$$

where $\mathcal{N} = (Nu/Nu_0)^{1/3}$ and $\alpha = \ln\mathcal{N}/\ln Re_0$.

In the ultimate regime and similarly to the classical regime case, the ratio Nu/Nu_0 is a function of the product $\tilde{l} \times Nu_0$. However, α also depends on the Rayleigh number through the Reynolds number Re_0. When $\tilde{l} \to 0$, $\alpha \approx 0$ since on the one hand $\mathcal{N} \to 1$ and on the other Reynolds numbers Re_0 must be large enough to reach the ultimate regime. The limit of (3.9) when $\tilde{l} \to 0$ is then given in Table 1. For large values of $\tilde{l}$, (3.9) can be solved numerically for each chosen couple (Ra,$\tilde{l}$) to obtain $\mathcal{N}$ and then Nu. At high Nu_0 or else at very high Rayleigh numbers, Nu scales asymptotically as Ra^2 *i.e.* with an exponent 2 well above 1/2 (see Table 1).

3.3. *Extension of the GL theory*

The balances of the turbulent kinetic energy and of the thermal variance give the following two exact relations (Shraiman & Siggia 1990; Grossmann & Lohse 2000):

$$\langle\epsilon_u\rangle = \frac{g\alpha}{h}\left[\int_0^h \frac{\overline{\Phi}(z)}{\rho c_p}\mathrm{d}z - \frac{\lambda\Delta T}{\rho c_p}\right], \tag{3.10}$$

$$\langle\epsilon_T\rangle = \frac{1}{h}\int_0^h \overline{T}(z)\frac{q_v(z)}{\rho c_p}\mathrm{d}z + \frac{T_h\,\overline{\Phi}(0) - T_c\,\overline{\Phi}(h)}{\rho c_p\, h}. \tag{3.11}$$

Actually, for a standard RB experiment, the convective flow is driven by the thermal boundary conditions (ΔT or $\overline{\Phi}(z{=}0)$) whereas for the modified RB experiment presented in Fig. 1, the volumetric power source controls the intensity of the convective flow. Besides, for the second case, the lower and upper plates are assumed to be perfectly insulated conducting to $\overline{\Phi}(0) = \overline{\Phi}(h) = 0$. In steady state, energy conservation yields to the following relation between the heat flux and volumetric power source:

$$\frac{\overline{\Phi}(z)}{Q} = \begin{cases} 1 - \exp\left(-\dfrac{z}{l}\right) & \text{for } z \leqslant h/2, \\ 1 - \exp\left(\dfrac{h-z}{l}\right) & \text{for } h/2 \leqslant z \leqslant h. \end{cases} \tag{3.12}$$

Using (3.12) and (1.2), and assuming $Nu \gg 1$, (3.10) becomes:

$$\langle \epsilon_u \rangle = \frac{\nu^3}{h^4} \frac{NuRa}{Pr^2} (1 - \mathcal{C}). \tag{3.13}$$

The corrective term $\mathcal{C} = 2\tilde{l}\left[1 - \exp\left(-\frac{1}{2\tilde{l}}\right)\right]$ only depends on $\tilde{l}$ and varies as $2\tilde{l}$ when $\tilde{l} \to 0$. Thus, the expression giving the dissipation rate of kinetic energy averaged over the whole cell (3.13) is very similar to that obtained for a standard RB experiment (2.8).

As for the thermal dissipation rate, its average over the cell is related to the profile of the mean temperature (Eq. 3.11). As the GL theory is based on Prandtl-Blasius-Pohlhausen laminar boundary layers (Grossmann & Lohse 2000), the mean temperature can be written as:

$$2\frac{\overline{T}(z) - T_b}{\Delta T} = \begin{cases} 1 - \Theta_P\left(\dfrac{z}{\delta_T}\right) & \text{for } z \leqslant h/2, \\ \Theta_P\left(\dfrac{h-z}{\delta_T}\right) - 1 & \text{for } h/2 \leqslant z \leqslant h, \end{cases} \tag{3.14}$$

with Θ_P the Pohlhausen temperature profile which is assumed to be independent of the Prandtl number. In particular, $\Theta_P(0) = 0$ and $\Theta_P(\eta) \to 1$ when $\eta \gg 1$. Using (3.14) and (1.1), (3.11) then becomes:

$$\langle \epsilon_T \rangle = \kappa \left(\frac{\Delta T}{h}\right)^2 Nu \frac{\delta_T}{l} \int_0^{h/(2\delta_T)} [1 - \Theta_P(\eta)] \exp\left(-\frac{\delta_T}{l}\eta\right) \mathrm{d}\eta. \tag{3.15}$$

Equation (3.15) shows that $\langle \epsilon_T \rangle$ depends both on $\tilde{l} = l/h$ and δ_T/h. The hypothesis adopted in sub-section 3.1 for extending the classical regime of Malkus is again adopted here (Eq. 3.4). δ_T/h is assumed to be only controlled by the Rayleigh number so that $\delta_T/h = 1/[2Nu_0(Ra)]$, where Nu_0 is the Nusselt number for a standard RB experiment. Equation (3.15) becomes:

$$\langle \epsilon_T \rangle = \kappa \left(\frac{\Delta T}{h}\right)^2 Nu\, \mathcal{G}(2Nu_0\tilde{l}), \tag{3.16}$$

with

$$\mathcal{G}(y) = \frac{1}{y} \int_0^{\infty} [1 - \Theta_P(\eta)] \exp\left(-\frac{\eta}{y}\right) \mathrm{d}\eta. \tag{3.17}$$

Then, the central idea of the GL theory is to split the dissipation rates into two contributions (see (2.10)-(2.13)). Generalisation of (2.15)-(2.17) are:

$$\langle \epsilon_u \rangle_{Bu} \sim \frac{U^2}{h/U}\left(1 - \frac{\delta_u}{h}\right) \approx \frac{\nu^3}{h^4} Re^3, \tag{3.18}$$

$$\langle \epsilon_T \rangle_{Bu} \sim \frac{(\Delta T)^2}{h/U^{edge}}\left(1 - \frac{\delta_T}{h}\right) \approx \kappa \left(\frac{\Delta T}{h}\right)^2 RePrf\left(\frac{2aNu_0}{\sqrt{Re}}\right), \tag{3.19}$$

$$\langle \epsilon_u \rangle_{BL} \sim \nu \left(\frac{U}{\delta_u}\right)^2 \frac{\delta_u}{h} = \frac{\nu^3}{h^4} \frac{Re^{5/2}}{2a}. \tag{3.20}$$

To obtain (3.19), the relevant velocity at the edge between the thermal BL and bulk is assumed to be expressed as $U^{edge} = Uf(\delta_u/\delta_T)$, with the same function f used for standard RB convection. Besides, we have

$$\frac{\delta_u}{\delta_T} = \frac{2Nu_0}{\sqrt{Re}}. \tag{3.21}$$

Combining (3.13) and (3.18), and using (2.5), we obtain the following first equation valid for both regimes II and IV:

$$\frac{Nu}{Nu_0}(1-\mathcal{C}) = \left(\frac{Re}{Re_0}\right)^3 \text{ (regimes } II \text{ and } IV). \tag{3.22}$$

Forgetting the corrective term $\mathcal{C}$ which must be small since $\tilde{l} \ll 1$, (3.22) is the same equation as the one obtained both for extending the classical and ultimate regimes of Malkus and Kraichnan (see Eq. 3.8). On the contrary, for regimes I and III, (3.22) needs to be replaced by:

$$\frac{Nu}{Nu_0}(1-\mathcal{C}) = \left(\frac{Re}{Re_0}\right)^{5/2} \text{ (regimes } I \text{ and } III). \tag{3.23}$$

The results of this theory is first presented for regime IV because most of the experimental and numerical results fall into this regime. In addition, unlike regime II, the extension of regime IV to internally heated convection does not require the introduction of any adjustable parameters.

3.3.1. *Regime IV, $\langle\epsilon_u\rangle \sim \langle\epsilon_u\rangle_{Bu}$ and $\langle\epsilon_T\rangle \sim \langle\epsilon_T\rangle_{Bu}$*

For regime IV, the thermal dissipation rate is dominated by its bulk contribution. Combining (3.16) and (3.19), and using (2.19), we obtain:

$$\frac{Nu}{Nu_0}\,\mathcal{G}(2Nu_0\tilde{l}) = \frac{Re}{Re_0}\frac{f(2aNu_0/\sqrt{Re})}{f(2aNu_0/\sqrt{Re_0})}. \tag{3.24}$$

The system of equations (3.22) and (3.24) gives the dependency of both Nu/Nu_0 and Re/Re_0 as a function of the 3 control parameters: Ra, Pr and $\tilde{l} = l/h$. For Prandtl numbers small or large enough, (3.24) can be simplified as follows:

$$\frac{Nu}{Nu_0} = \begin{cases} (1-\mathcal{C})^{-\frac{1}{2}}\left[\mathcal{G}(2Nu_0\tilde{l})\right]^{-\frac{3}{2}}, & \text{for } \delta_T \gg \delta_u \quad (\text{regime } IV_l) \qquad (3.25a) \\ (1-\mathcal{C})\left[\mathcal{G}(2Nu_0\tilde{l})\right]^{-2}, & \text{for } \delta_u \gg \delta_T \quad (\text{regime } IV_u). \qquad (3.25b) \end{cases}$$

Besides, the limits of (3.25a) and (3.25b) when $\tilde{l}Nu_0$ tends to 0 or ∞ can be obtained saying that $\mathcal{G}(y) \overset{y\to 0}{\approx} 1 - \Theta_P'(0)y$ or $\mathcal{G}(y) \overset{y\to\infty}{\approx} \delta_\Theta^d/y$, where $\delta_\Theta^d = \int_0^\infty [1-\theta_P(\eta)]\mathrm{d}\eta$. A summary of the corresponding results is given in Table 1.

3.3.2. *Regime II, $\langle\epsilon_u\rangle \sim \langle\epsilon_u\rangle_{Bu}$ and $\langle\epsilon_T\rangle \sim \langle\epsilon_T\rangle_{BL}$*

Following the idea of Grossmann & Lohse (2000), we consider the order of magnitude of the different terms of energy equation i.e. $u_x\partial_x T + u_z\partial_z T = \kappa\partial_{zz}T + \frac{q_v}{\rho c_p}$. It yields to

$$\frac{U^{edge}\Delta T}{h} \sim \frac{\kappa\Delta T}{\delta_T^2} + A\frac{q_v(\delta_T)}{\rho c_p}. \tag{3.26}$$

Using (1.1), (1.2), (2.1), (2.21) and $U^{edge} = Uf(\delta_u/\delta_T)$, (3.26) becomes:

$$1 + \tilde{A}\frac{Nu}{Nu_0}\mathcal{H}(2Nu_0\tilde{l}) = \frac{Re}{Re_0}\frac{f(2aNu_0/\sqrt{Re})}{f(2aNu_0/\sqrt{Re_0})}, \tag{3.27}$$

with $\mathcal{H}(y) = \frac{1}{y}\exp\left(-\frac{1}{y}\right)$, $0 \leqslant \mathcal{H}(y) \leqslant \exp(-1) \approx 0.37$, and $\tilde{A}$ a numerical constant of the order of one to be determined experimentally.

	Nu_0	$\frac{Nu}{Nu_0}-1$ for $\tilde{l}\,Nu_0 \ll 1$	Nu for $\tilde{l}\,Nu_0 \gg 1$
Classical regime by Malkus, Eq. (3.5)	$\sim Ra^{\frac{1}{3}}$	$2\,\tilde{l}\,Nu_0$ $\sim \tilde{l}\,Ra^{\frac{1}{3}}$	$4\,\tilde{l}\,Nu_0^2$ $\sim \tilde{l}\,Ra^{\frac{2}{3}}$
Ultimate regime by Kraichnan, Eq. (3.9)	$\sim (C_0^{\mathcal{U}}Ra)^{\frac{1}{2}}$	$3\,\tilde{l}\,Nu_0$ $\sim \tilde{l}\,(C_0^{\mathcal{U}}Ra)^{\frac{1}{2}}$	$(\frac{2}{1+\alpha})^6\ \tilde{l}^3\,Nu_0^4$ $\sim\ \tilde{l}^3\,(C_0^{\mathcal{U}}\,Ra)^2$
Regime IV_l by GL, Eq. (3.25a)	$\sim (RaPr)^{\frac{1}{2}}$	$3\Theta_P'(0)\,\tilde{l}\,Nu_0$ $\sim \tilde{l}(RaPr)^{\frac{1}{2}}$	$\left(\frac{2}{\delta_\Theta^d}\right)^{3/2}\ \tilde{l}^{\frac{3}{2}}\,Nu_0^{\frac{5}{2}}$ $\sim \tilde{l}^{\frac{3}{2}}\,(RaPr)^{\frac{5}{4}}$
Regime IV_u by GL, Eq. (3.25b)	$\sim Ra^{\frac{1}{3}}$	$4\Theta_P'(0)\,\tilde{l}\,Nu_0$ $\sim \tilde{l}\,Ra^{\frac{1}{3}}$	$\left(\frac{2}{\delta_\Theta^d}\right)^{2}\ \tilde{l}^2\,Nu_0^3$ $\sim\ \tilde{l}^2\,Ra$
Regime III_u by GL, Eq. (3.30)	$\sim Ra^{\frac{3}{7}}Pr^{-\frac{1}{7}}$	$5\Theta_P'(0)\,\tilde{l}\,Nu_0$ $\sim \tilde{l}\,Ra^{\frac{3}{7}}Pr^{-\frac{1}{7}}$	$\left(\frac{2}{\delta_\Theta^d}\right)^{\frac{5}{2}}\ \tilde{l}^{\frac{5}{2}}\,Nu_0^{\frac{7}{2}}$ $\sim\ \tilde{l}^{\frac{5}{2}}\,Ra^{\frac{3}{2}}Pr^{-\frac{1}{2}}$

TABLE 1. Limits when $\tilde{l}\,Nu_0 \ll 1$ and $\tilde{l}\,Nu_0 \gg 1$ of the Nusselt number for a radiatively heated convection experiment. For the ultimate regime by Kraichnan, $\alpha = \ln(Nu/Nu_0)/(3\ln Re_0)$ and $C_0^{\mathcal{U}} = Pr/(Pe^*\ln Re_0)^3$. For regimes IV and III by GL, we assume that $\tilde{l} \ll 1$ to have $\mathcal{C} \to 0$.

Equations (3.22) and (3.27) give the dependency of both Nu/Nu_0 and Re/Re_0 as a function of Ra, Pr and $\tilde{l} = l/h$. Contrary to the regime IV, Re/Re_0 and Nu/Nu_0 both tend towards 1 when $Nu_0\tilde{l} \gg 1$ for regime II because $\mathcal{H}(y) \approx 1/y$ when $y \gg 1$. For the two limits $Nu_0\tilde{l} \ll 1$ and $Nu_0\tilde{l} \gg 1$, we obtain:

$$\frac{Nu}{Nu_0}(1-\mathcal{C}) = 1 + \frac{\tilde{A}\,\theta_i}{1-\mathcal{C}}\mathcal{H}(2Nu_0\tilde{l}), \tag{3.28}$$

with $\theta_i = 3$ for $\delta_T \gg \delta_u$ (regime II_l) and $\theta_i = 2$ for $\delta_u \gg \delta_T$ (regime II_u).

For any value of $Nu_0\tilde{l}$, we show in appendix A that Nu/Nu_0 can be given with a very good approximation by:

$$\frac{Nu}{Nu_0}(1-\mathcal{C}) = \left[\mathcal{S}_{\beta_0}\left(\frac{\tilde{A}\,\mathcal{H}}{1-\mathcal{C}}\right)\right]^3, \tag{3.29}$$

with $\mathcal{S}_\beta(x)$ the real and positive solution of the equation: $1 + x\mathcal{S}_\beta^3 = \mathcal{S}_\beta^{1+\beta/2}$, and $\beta_0 = \left[\frac{2aNu_0}{\sqrt{Re_0}}f(\frac{2aNu_0}{\sqrt{Re_0}})\right]^{-n}$.

3.3.3. *Regime I, $\langle\epsilon_u\rangle \sim \langle\epsilon_u\rangle_{BL}$ and $\langle\epsilon_T\rangle \sim \langle\epsilon_T\rangle_{BL}$*

For regime I, (3.23) and (3.27) give Nu/Nu_0 and Re/Re_0 as a function of Ra, Pr and $\tilde{l} = l/h$. For the two limits $Nu_0\tilde{l} \ll 1$ and $Nu_0\tilde{l} \gg 1$, (3.28) is valid with $\theta_i = 5/2$ for $\delta_T \gg \delta_u$ (regime I_l) and $\theta_i = 5/3$ for $\delta_u \gg \delta_T$ (regime I_u).

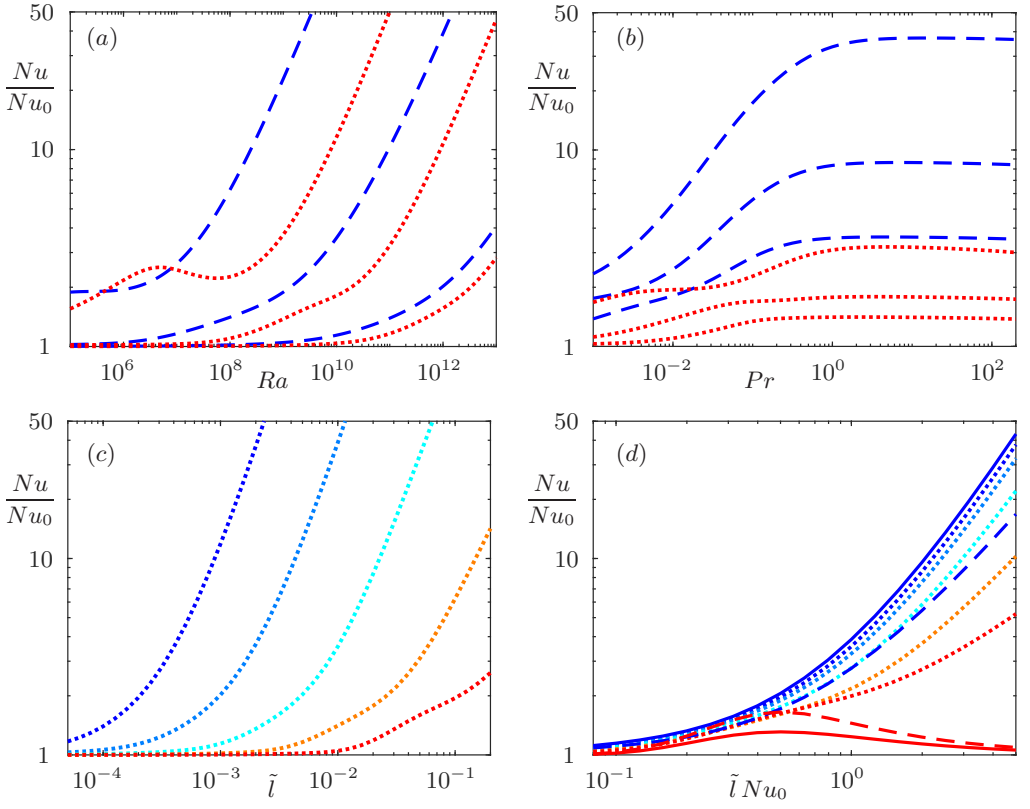

FIGURE 2. Results of the extension of GL theory for radiatively heated convection using (3.33) and (3.34) with $\tilde{A} = 0.3$. The coefficient a and prefactors c_1-c_4 are given by Stevens *et al.* (2013). (*a*) Nu/Nu_0 versus Ra for $Pr = 0.01$ (red dotted lines) and $Pr = 1$ (blue dashed lines), and for $\tilde{l} = 10^{-3}$ (lowest line), $\tilde{l} = 10^{-2}$ (middle line) and $\tilde{l} = 0.1$ (highest line). (*b*) Nu/Nu_0 versus Pr for $Ra = 10^8$ (red dotted lines) and $Ra = 10^{10}$ (blue dashed lines), and for $\tilde{l} = 0.01$ (lowest line), $\tilde{l} = 0.02$ (middle line) and $\tilde{l} = 0.05$ (highest line). (*c*) Nu/Nu_0 versus $\tilde{l}$ for $Pr = 1$ and for $Ra = 10^6$ (lowest line), 10^8, 10^{10}, 10^{12} and 10^{14} (highest line). (*d*) Same results as (*c*) but using $\tilde{l} \times Nu_0$ as x-coordinate. Also shown: regime IV_u ($Nu/Nu_0 = \mathcal{G}^{-2}$) (blue solid line), regime IV_l ($Nu/Nu_0 = \mathcal{G}^{-3/2}$) (blue dashed line), regime II_u (red solid line) and regime II_l (red dashed line).

3.3.4. *Regime III, $\langle \epsilon_u \rangle \sim \langle \epsilon_u \rangle_{BL}$ and $\langle \epsilon_T \rangle \sim \langle \epsilon_T \rangle_{Bu}$*

For regime III, (3.23) and (3.24) give Nu/Nu_0 and Re/Re_0 as a function of Ra, Pr and $\tilde{l} = l/h$. For Prandtl numbers large enough, we obtain:

$$\frac{Nu}{Nu_0} = (1 - \mathcal{C}_u)^{3/2} \left[\mathcal{G}(2Nu_0\tilde{l})\right]^{-5/2} \quad \text{for } \delta_u \gg \delta_T \quad (\text{regime } III_u). \tag{3.30}$$

The limits of (3.30) when $\tilde{l} \times Nu_0$ tends to 0 or ∞ are given in Table 1.

3.3.5. *Theory in the whole parameter $(Ra, Pr, \tilde{l})$ plane*

Following the idea of Grossmann & Lohse (2001) (see paragraph 2.3.3), at given Ra, Pr and $\tilde{l}$, radiatively driven convection can be described as a mixture of these 4 regimes. By replacing the expressions of $\langle \epsilon_u \rangle_{Bu}$ (3.18) and $\langle \epsilon_u \rangle_{BL}$ (3.20) in the balance equation

for the viscous dissipation rate (3.13), the first generalised equation can be written as:

$$\frac{RaNu}{Pr^2}(1-\mathcal{C}) = c_1\frac{Re^{5/2}}{2a} + c_2 Re^3. \tag{3.31}$$

Using (3.24) and (3.29), the second generalised equation becomes:

$$Nu = \frac{c_3}{1-\mathcal{C}}\left[\mathcal{S}_\beta\left(\frac{\tilde{A}\,\mathcal{H}}{1-\mathcal{C}}\right)\right]^3\sqrt{Re_0 Prf\left(\frac{2aNu_0}{\sqrt{Re_0}}\right)} + \frac{c_4}{\mathcal{G}}RePrf\left(\frac{2aNu_0}{\sqrt{Re}}\right). \tag{3.32}$$

By combining on the one hand (2.27) and (3.31), and on the other hand (2.28) and (3.32), we obtain the two equations which give Nu and Re numbers as a function of the 3 parameters Ra, Pr and $\tilde{l}$:

$$\frac{Nu}{Nu_0} = \frac{1}{1-\mathcal{C}}\frac{c_1\frac{Re^{5/2}}{2a} + c_2 Re^3}{c_1\frac{Re_0^{5/2}}{2a} + c_2 Re_0^3}, \tag{3.33}$$

$$\frac{Nu}{Nu_0} = \frac{\frac{c_3}{1-\mathcal{C}}\left[\mathcal{S}_\beta\left(\frac{\tilde{A}\,\mathcal{H}}{1-\mathcal{C}}\right)\right]^3\sqrt{Re_0 Prf\left(\frac{2aNu_0}{\sqrt{Re_0}}\right)} + \frac{c_4}{\mathcal{G}}RePrf\left(\frac{2aNu_0}{\sqrt{Re}}\right)}{c_3\sqrt{Re_0 Prf\left(\frac{2aNu_0}{\sqrt{Re_0}}\right)} + c_4 Re_0 Prf\left(\frac{2aNu_0}{\sqrt{Re_0}}\right)}. \tag{3.34}$$

Figures 2 (*a*) and (*b*) show the variations of the ratio Nu/Nu_0 against Ra and Pr for fixed values of $\tilde{l}$, while Nu/Nu_0 is plotted against $\tilde{l}$ in Fig. 2 (*c*) for $Pr = 1$ and for fixed values of Ra between 10^6 and 10^{14}. As observed previously for the extensions of Malkus and Kraichnan theories, the use of the variable $Nu_0 \times \tilde{l}$ allows to gather the various curves drawn in Fig. 2 (*c*) (see Fig. 2*d*). As underlined by Grossmann & Lohse (2001) for RB convection, pure regime IV_u is only reached for very high Ra and Pr numbers (blue upper solid line in Fig. 2*d*) while for moderate values of Ra and Pr numbers, radiatively heated convection is described by a mixing of the 4 regimes I-IV.

4. Comparison with experimental results

The predictions of this theoretical approach can be tested thanks to the recent experimental investigation of Lepot *et al.* (2018); Bouillaut *et al.* (2019). The measurements cover a range of 4×10^6 to 4×10^9 for Ra, 5×10^{-5} to 0.1 for $\tilde{l} = l/h$ and the working fluid was water so the Prandtl number was set at a constant value close to 7. Here, the Rayleigh and Nusselt numbers are defined using $\Delta T = 2(T_h - T_b)$, where T_h and T_b are the measured temperature of the lower plate and the bulk flow, respectively. Hence, there is a factor 2 for Ra (and a factor 1/2 for Nu) by comparing the figures from Lepot *et al.* (2018); Bouillaut *et al.* (2019) and with those presented here. Instead of plotting Nu as a function of Ra, the theory presented in section 3 shows that Nusselt numbers for various $\tilde{l}$ should better collapse around a single curve by plotting the ratio of the Nusselt numbers for modified and standard RB experiments (Nu/Nu_0) against the product of $\tilde{l}$ and Nu_0. As underlined by Lepot *et al.* (2018); Bouillaut *et al.* (2019), their experiments converge to RB experiments when $\tilde{l} \to 0$, even though the boundary conditions are very different (the horizontal plates are insulated while they are perfectly conductive for RB convection). Indeed, for $\tilde{l} = 5 \times 10^{-5}$, Nusselt numbers given by Bouillaut *et al.* (2019) can be fitted by a simple scaling such as $Nu = 0.076 \times Ra^{1/3}$ with a maximum deviation of 7%, or by the GL theory with $a = 0.75$, $c_1 = 8.05$, $c_2 = 1.38$, $c_3 = 0.3$ and $c_4 = 0.03$. Prefactors c_1 and c_2 are the ones given by Stevens *et al.* (2013) while c_3 and c_4 are slightly modified to better fit to the experimental results (Stevens *et al.* (2013) advocated taking

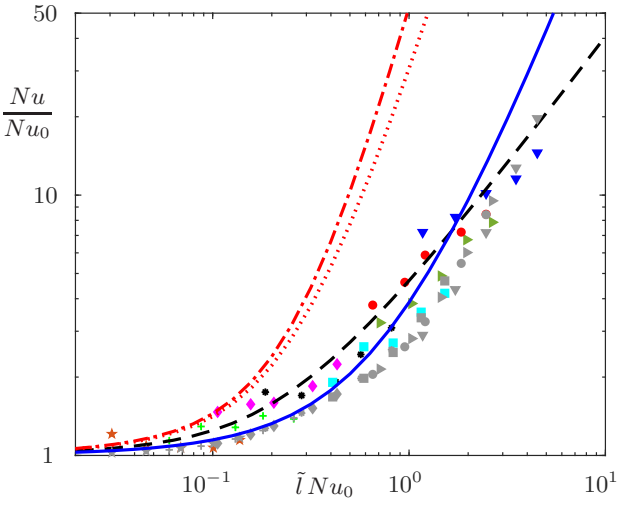

FIGURE 3. Compensated Nusselt numbers for a radiatively heated convection experiment as a function of $\tilde{l}\,Nu_0$. Coloured symbols: experiments from Bouillaut *et al.* (2019) with $\tilde{l} = 0.0015$ ($\star$), $\tilde{l} = 0.003$ ($+$), $\tilde{l} = 0.006$ ($\diamond$), $\tilde{l} = 0.0012$ ($*$), $\tilde{l} = 0.0024$ ($\square$), $\tilde{l} = 0.048$ ($\triangleright$), $\tilde{l} = 0.05$ ($\circ$), $\tilde{l} = 0.096$ (∇). Black dashed line: extension of the classical regime by Malkus (1954), Eq. (3.5), no adjustable parameter. Blue solid line: extension of the classical regime IV_u by Grossmann & Lohse (2000), Eq. (3.25*b*) with $\mathcal{C} = 0$, no adjustable parameter. Grey symbols: Eqs. (3.33) and (3.34) with $\tilde{A} = 0.35$. Upper red lines: extension of the ultimate regime by Kraichnan (1962), Eq. (3.9) with $Re_0 = 1000$ (red dotted line) and $Re_0 = 10^{10}$ (red dashed line).

$c_3 = 0.487$ and $c_4 = 0.0252$). Using GL theory for defining Nu_0, the experimental results of Bouillaut *et al.* (2019) are plotted in Fig. 3 for $0.0015 \leqslant \tilde{l} \leqslant 0.01$ (coloured symbols). The black dashed and blue solid lines represent, respectively, the extension of the classical scaling proposed by Malkus (1954) (Eq. 3.5) and the extension of regime IV_u proposed by Grossmann & Lohse (2000) (Eq. 3.25*b*). First, instead of plotting Nu against Ra (see Fig. 2 in Bouillaut *et al.* (2019)), plotting compensated Nusselt numbers Nu/Nu_0 as a function of $\tilde{l}\,Nu_0 \sim \tilde{l}\,Ra^{1/3}$ allows to collapse the experimental data on a single curve. Secondly, this curve is given by (3.5) or (3.25*b*) with a fairly good accuracy and without the use of any adjustable parameter. The system of equations (3.33) and (3.34) that results from a mixture of regimes I to IV and is represented by grey symbols in Fig. 3 gives slightly lower values for the ratio Nu/Nu_0 than the pure regime IV (blue solid line). The new parameter $\tilde{A}$ has little impact on the curve for this data set and is fixed to 0.35 in Fig. 3. In view of: (i) the experimental uncertainties, (ii) the product $\tilde{l} \times Nu_0$ is always less than 5 and (iii) Pr number is fixed to 7 for the experimental results, it is difficult to discriminate between the different extensions of the theoretical models presented in section 3 describing convection in classical regimes.

On the contrary, it is well known that convection in the so-called ultimate regime behaves very differently since Nu_0 scales asymptotically as $Ra^{1/2}$, thus with an exponent 1/2 much higher than 1/3. The theoretical work presented in section 3 shows that, for radiatively heated convection, there is also a clear difference for the ratio Nu/Nu_0 between classical regimes and the ultimate regime. In figure 3, the two upper red lines represent the ultimate regime (Eq. 3.9) for two fixed Reynolds numbers (dotted line: $Re_0 = 1000$, dashed line: $Re_0 = 10^{10}$). They are clearly above all other curves and symbols describing the theoretical and experimental results for classical regimes. Indeed, Ra numbers achieved by the experiments of Bouillaut *et al.* (2019) are not sufficient to trigger the ultimate regime (a detailed discussion is given in appendix B).

5. Conclusions

The well known theories of RB convection have been extended here to radiatively heated convection. The evolution of the Nusselt number as a function of Ra, Pr and l/h (where l is the heating length near the lower plate and h the height of the cell) is predicted whatever the convection regime considered. In the classical regime and using the simple theory of Malkus (1954), equation (3.5) gives Nu/Nu_0 as a function of Ra and l/h without adjustable parameter, while, considering the more recent Grossmann & Lohse (2000) theory, the two equations (3.33) and (3.34) give the dependency of both Nu/Nu_0 and Re/Re_0 as a function of the 3 control parameters Ra, Pr and l/h. It can be noted that only the extension of regimes I and II of the GL theory, observable only at low Ra numbers, needs an adjustable parameter. A good agreement is observed between the experimental results obtained by Bouillaut *et al.* (2019) and the theoretical results for the classical regime. For the ultimate regime, equation (3.9) gives the Nusselt number as a function of Ra and l/h without adjustable parameter, but, in this case, no experimental or numerical results exist to test this prediction. Finally, this work predicts that the Nusselt number behaves asymptotically as $Ra^{2/3}$ or Ra for the classical regime (see Table 1) while it scales as Ra^2 in the ultimate regime, and this prediction is of major interest for geophysical and astrophysical flows where convection is driven by internal heat sources.

Acknowledgements

Bernard Castaing is gratefully thanked for his suggestions and the review of the article.

Declaration of interests

The author reports no conflict of interest.

Appendix A. Extension of regime II of the GL theory

For regime II, Eqs. (3.22) and (3.27) give the dependency of both Nu/Nu_0 and Re/Re_0 as a function of Ra, Pr and $\tilde{l} = l/h$. Using (3.22), (3.27) becomes:

$$1 + \frac{\tilde{A}\,\mathcal{H}}{1-\mathcal{C}}\left(\frac{Re}{Re_0}\right)^3 = \frac{Re}{Re_0}\frac{f\left(\frac{2aNu_0}{\sqrt{Re}}\right)}{f\left(\frac{2aNu_0}{\sqrt{Re_0}}\right)}. \tag{A 1}$$

A.1. *Regime II_u (high Pr numbers or $\delta_u \gg \delta_T$)*

Equation (A 1) becomes:

$$1 + \frac{\tilde{A}\,\mathcal{H}}{1-\mathcal{C}}\left(\frac{Re}{Re_0}\right)^3 = \left(\frac{Re}{Re_0}\right)^{3/2}. \tag{A 2}$$

To get a positive value for Re, we must have: $\tilde{A}\mathcal{H} \leqslant (1-\mathcal{C})/4 \leqslant 1/4$. As $\mathcal{H} \leqslant \exp(-1)$, the parameter $\tilde{A}$ needs to be lower than $\exp(1)/4 \approx 0.68$. Resolution of (A 2) gives:

$$\frac{Re}{Re_0} = \mathcal{S}_u\left(\frac{\tilde{A}\,\mathcal{H}}{1-\mathcal{C}}\right), \tag{A 3}$$

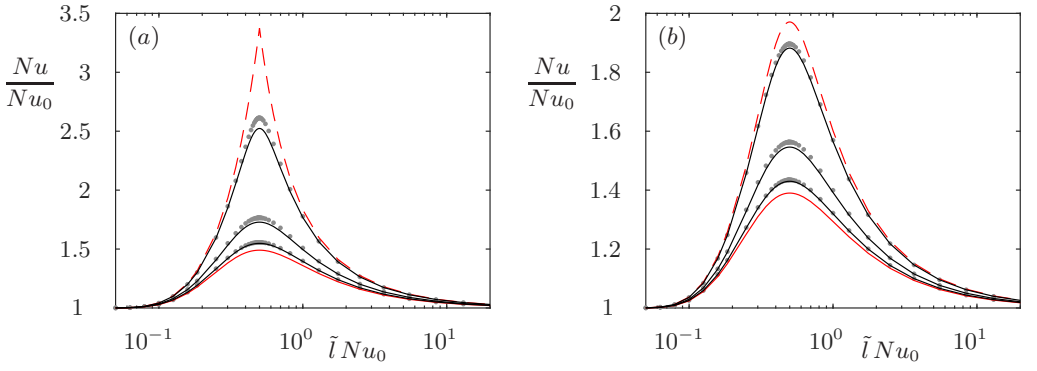

FIGURE 4. Nu/Nu_0 versus $\tilde{l}\,Nu_0$ in the regime II of the extension of GL theory for radiatively heated convection. Grey symbols: solution of Eqs. (3.22) and (3.27) with $\mathcal{C} = 0$, $\tilde{A} = 4\exp(1)/27 \approx 0.40$ (a) and $\tilde{A} = 0.35$ (b). Black solid lines: Eq. (3.29). From top to bottom, the parameter $2aNu_0/\sqrt{Re_0}$ is taken equal to 0.5, 1 and 1.5. The lower solid red line represents regime II_u while the upper dashed red line shows regime II_l.

with $\mathcal{S}_u(x) = \left(\dfrac{1-\sqrt{1-4x}}{2x}\right)^{2/3}$. $\mathcal{S}_u(x)$ is an increasing function of x with $\mathcal{S}_u(0) = 1$ and $\mathcal{S}_u(1/4) = 2^{2/3} \approx 1.59$, yielding to $1 \leqslant Re/Re_0 \leqslant 1.59$.

A.2. *Regime II_l (low Pr numbers or $\delta_T \gg \delta_u$)*

Equation (A 1) becomes:

$$1 + \frac{\tilde{A}\,\mathcal{H}}{1-\mathcal{C}}\left(\frac{Re}{Re_0}\right)^3 = \frac{Re}{Re_0}. \tag{A 4}$$

To get a positive value for Re, we must have: $\tilde{A}\mathcal{H} \leqslant 4(1-\mathcal{C})/27 \leqslant 4/27$. As $\mathcal{H} \leqslant \exp(-1)$, the parameter $\tilde{A}$ needs to be lower than $4\exp(1)/27 \approx 0.40$. Resolution of (A 4) gives:

$$\frac{Re}{Re_0} = \mathcal{S}_l\left(\frac{\tilde{A}\,\mathcal{H}}{1-\mathcal{C}}\right), \tag{A 5}$$

with $\mathcal{S}_l(x) = \dfrac{2}{\sqrt{3x}}\cos\left[\dfrac{1}{3}\arccos\left(\dfrac{3\sqrt{3x}}{2}\right) + \dfrac{\pi}{3}\right]$. $\mathcal{S}_l(x)$ is an increasing function of x with $\mathcal{S}_l(0) = 1$ and $\mathcal{S}_l(4/27) = 3/2$ yielding to $1 \leqslant Re/Re_0 \leqslant 3/2$.

A.3. *Approximation of (A 1) for any Pr numbers*

For the two limits $Pr \gg 1$ and $Pr \ll 1$, we have shown that $1 \leqslant Re/Re_0 \leqslant 3/2$. The following approximation can then be adopted: $f(x_0) \approx f(x)(\frac{x}{x_0})^{-\beta_0}$, with $\beta_0 = -\left(\frac{\mathrm{d}\ln f}{\mathrm{d}\ln x}\right)_{x=x_0} = [x_0 f(x_0)]^{-n}$ $(n = 4)$. When $x_0 \gg 1$, $\beta_0 \to 3/2$ while $\beta_0 \to 0$ when $x_0 \to 0$. Equation (A 1) can therefore be approximated by:

$$1 + \frac{\tilde{A}\,\mathcal{H}}{1-\mathcal{C}}\left(\frac{Re}{Re_0}\right)^3 = \left(\frac{Re}{Re_0}\right)^{1+\beta_0/2}. \tag{A 6}$$

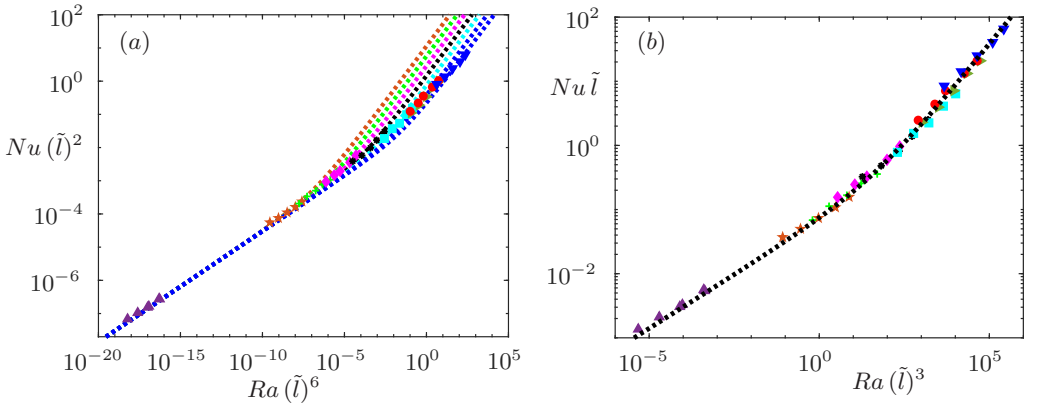

FIGURE 5. Comparison of the scaling proposed by Bouillaut *et al.* (2019) (*a*) and the model described in section 3 (*b*). Symbols as in Fig. 3. Dotted lines: (3.5), without adjustable parameter.

By calling $\mathcal{S}_\beta(x)$ the real and positive solution of the equation: $1 + x\mathcal{S}_\beta^3 = \mathcal{S}_\beta^{1+\beta/2}$, we obtain:

$$\frac{Re}{Re_0} = \mathcal{S}_{\beta_0}\left(\frac{\tilde{A}\,\mathcal{H}}{1-\mathcal{C}}\right), \tag{A 7}$$

with $\beta_0 = \left[\frac{2aNu_0}{\sqrt{Re_0}} f(\frac{2aNu_0}{\sqrt{Re_0}})\right]^{-n}$. Using (A 7), (3.22) gives the variations of Nu/Nu_0 as a function of Ra, Pr and $\tilde{l}$ in the regime II (Eq. 3.29). These variations are plotted in Fig. 4 (*a*) with $\tilde{A} = 4\exp(1)/27 \approx 0.40$ and in Fig. 4 (*b*) with $\tilde{A} = 0.35$. For each case, we can note that Eq. (3.29) (represented by black solid lines) is a good approximation of the solution of the system of Eqs. (3.22) and (3.27) (grey symbols). That is why (3.29) is used in sub-section 3.3.5 to extent GL theory to radiatively heated convection in the whole parameter $(Ra, Pr, \tilde{l})$ plane.

Appendix B. Discussion of the model and scaling proposed by Bouillaut *et al.* (2019)

Bouillaut *et al.* (2019) proposed a simple model to describe radiatively driven convection leading to the scaling relation $Nu \sim \tilde{l}\,(RaPr)^{1/2}$. The theory presented in section 3 shows that the scaling $Nu \sim Ra^{1/2}$ can only be observed for a limited range of Ra for each $\tilde{l}$ considered. Indeed, using for example Eq. (3.5), Nu scales as $Ra^{1/3}$ when $\tilde{l} \to 0$ while it scales as $Ra^{2/3}$ when $\tilde{l} \times Ra^{1/3}$ is quite high. Thus, for a limited range of Ra, Nu can be fitted by $Ra^{1/2}$ but this scaling cannot be observed asymptotically. Bouillaut *et al.* (2019) have also proposed to represent the experimental data considering the product of Nu and $\tilde{l}^2$ as a function of the product of Ra and $\tilde{l}^6$ (see Fig. 5*a*). The theory presented here shows that, in this representation, the experimental data can only collapse on a single curve if both the range of Ra is relatively small and this range is the same for all the $\tilde{l}$ investigated. On the contrary, (3.5) predicts that $Nu\,\tilde{l}$ depends only on $Nu_0\,\tilde{l}$ or only on $Ra\,\tilde{l}^3$ with assuming $Nu_0 \sim Ra^{1/3}$ (Eq. 2.3). Besides, in this representation (Fig. 5*b*), the curve is given by (3.5) and without any adjustable parameter.

REFERENCES

Ahlers, G., Grossmann, S. & Lohse, D. 2009 Heat transfer and large scale dynamics in turbulent Rayleigh-Bénard convection. *Rev. Mod. Phys.* **81**, 503–537.

Bouillaut, V., Lepot, S., Aumaître, S. & Gallet, B. 2019 Transition to the ultimate regime in a radiatively driven convection experiment. *J. Fluid Mech.* **861**, R5.

Chavanne, X., Chillà, F., Castaing, B., Hébral, B., Chabaud, B. & Chaussy, J. 1997 Observation of the ultimate regime in Rayleigh-Bénard convection. *Phys. Rev. Lett.* **79**, 3648–3651.

Chillà, F & Schumacher, J. 2012 New perspectives in turbulent Rayleigh-Bénard convection. *Eur. Phys. J. E* **35**, 58.

Doering, C. R. 2019 Thermal forcing and classical and ultimate regimes of Rayleigh-Bénard convection. *J. Fluid Mech.* **868**, 1–4.

Goluskin, D. 2015 *Internally Heated Convection and Rayleigh-Bénard Convection*. Springer.

Goluskin, D. & van der Poel, E. P. 2016 Penetrative internally heated convection in two and three dimensions. *J. Fluid Mech.* **791**, R6.

Grossmann, S. & Lohse, D. 2000 Scaling in thermal convection: A unifying view. *J. Fluid Mech.* **407**, 27–56.

Grossmann, S. & Lohse, D. 2001 Thermal convection for large Prandtl numbers. *Phys. Rev. Lett.* **86**, 3316–3319.

Grossmann, S. & Lohse, D. 2011 Multiple scaling in the ultimate regime of thermal convection. *Phys. Fluids* **23** (4), 045108.

Kraichnan, R. H. 1962 Turbulent thermal convection at arbitrary Prandtl number. *Phys. Fluids* **5** (11), 1374–1389.

Kulacki, F. A. & Goldstein, R. J. 1972 Thermal convection in a horizontal fluid layer with uniform volumetric energy sources. *J. Fluid Mech.* **55** (2), 271–287.

Lepot, S., Aumaître, S. & Gallet, B. 2018 Radiative heating achieves the ultimate regime of thermal convection. *Proc. Natl Acad. Sci. USA* **115**, 8937–8941.

Malkus, W. V. R. 1954 The heat transport and spectrum of thermal turbulence. *Proc. Roy. Soc. A* **225**, 196–212.

Priestley, C. H. B. 1954 Convection from a large horizontal surface. *Aust. J. Phys.* **7**, 176–201.

Qiu, X.-L., Xia, K.-Q. & Tong, P. 2005 Experimental study of velocity boundary layer near a rough conducting surface in turbulent natural convection. *J. Turbul.* **6**, 30.

Roche, P.-E., Castaing, B., Chabaud, B. & Hébral, B. 2001 Observation of the 1/2 power law in Rayleigh-Bénard convection. *Phys. Rev. E* **63** (4), 045303.

Rusaouën, E., Liot, O., Castaing, B., Salort, J. & Chillà, F. 2018 Thermal transfer in Rayleigh-Bénard cell with smooth or rough boundaries. *J. Fluid Mech.* **837**, 443–460.

Shen, Y., Tong, P. & Xia, K.-Q. 1996 Turbulent convection over rough surfaces. *Phys. Rev. Lett.* **76**, 908–911.

Shraiman, B. I. & Siggia, E. D. 1990 Heat transport in high-Rayleigh number convection. *Phys. Rev. A* **42**, 3650–3653.

Siggia, E. D. 1994 High rayleigh number convection. *Ann. Rev. Fluid Mech.* **26** (1), 137–168.

Spiegel, E. A. 1971 Convection in stars I. Basic Boussinesq convection. *Annu. Rev. Astron. Astrophys.* **9** (1), 323–352.

Stevens, R. J. A. M., van der Poel, E. P., Grossmann, S. & Lohse, D. 2013 The unifying theory of scaling in thermal convection: the updated prefactors. *J. Fluid Mech.* **730**, 295–308.

Stringano, G., Pascazio, G. & Verzicco, R. 2006 Turbulent thermal convection over grooved plates. *J. Fluid Mech.* **557**, 307–336.

Tisserand, J.-C., Creyssels, M., Gasteuil, Y., Pabiou, H., Gibert, M., Castaing, B. & Chillà, F. 2011 Comparison between rough and smooth plates within the same Rayleigh-Bénard cell. *Phys. Fluids* **23** (1), 015105.

Zhu, X., Stevens, R. J. A. M., Shishkina, O., Verzicco, R. & Lohse, D. 2019 $Nu \sim Ra^{1/2}$ scaling enabled by multiscale wall roughness in Rayleigh-Bénard turbulence. *J. Fluid Mech.* **869**, R4.

Zhu, X., Stevens, R. J. A. M., Verzicco, R. & Lohse, D. 2017 Roughness-facilitated local 1/2 scaling does not imply the onset of the ultimate regime of thermal convection. *Phys. Rev. Lett.* **119**, 154501.